Spectrally resolved femtosecond two-color three-pulse photon echoes: Study of ground and excited state dynamics in molecules

Lap Van Dao,[a] Craig Lincoln, Martin Lowe, and Peter Hannaford
Centre for Atom Optics and Ultrafast Spectroscopy, School of Biophysical Sciences and Electrical Engineering, Swinburne University of Technology, Melbourne, Australia 3122

(Received 9 July 2003; accepted 8 January 2004)

We report the use of spectrally resolved femtosecond two-color three-pulse photon echoes as a potentially powerful multidimensional technique for studying vibrational and electronic dynamics in complex molecules. The wavelengths of the pump and probe laser pulses are found to have a dramatic effect on the spectrum of the photon echo signal and can be chosen to select different sets of energy levels in the vibrational manifold, allowing a study of the dynamics and vibrational splitting in either the ground or the excited state. The technique is applied to studies of the dynamics of vibrational electronic states in the dye molecule Rhodamine 101 in methanol. © *2004 American Institute of Physics.* [DOI: 10.1063/1.1651057]

I. INTRODUCTION

The aim of femtosecond nonlinear coherent spectroscopy in molecules[1–8] is to determine various nonlinear optical responses that reflect the dynamics of the inter- and intramolecular motion and to construct physical models of the underlying dynamical processes. Time-resolved infrared spectroscopy[5,6] provides a means of directly accessing such vibrational dynamics in the electronic ground state and can provide complementary information to Raman spectroscopy. However these techniques are difficult to apply to excited electronic states and to complex molecules. Femtosecond pump–probe techniques such as transient absorption[9] suffer from the difficulty of interpreting the data at very short times where overlap of the pulses results in a coherence spike feature. A similar problem arises with conventional femtosecond photon echo techniques such as photon echo peak shift measurements,[2] where the initial time behavior of the correlation function is masked by the rapid free induction decay of the inhomogeneously broadened system. For complex molecules much of the interesting dynamics occurs at very short times during the pulse overlap thus making it difficult to selectively excite a single band in a crowded spectrum and to follow the dynamics which give rise to the spectral width of the band.

To improve the capability of femtosecond nonlinear spectroscopy experiments, more than two laser pulses have been used.[2,7,8,10–13] The multiple laser pulses create a nonlinear polarization involving wave packets of molecular states and establish a definite phase relationship (or coherence) between the different states. The laser pulses can manipulate and probe this coherence, which is strongly dependent on the molecular structure, electronic vibrational coupling mechanisms, and the molecular environment. By measuring the nonlinear polarization in the time domain, detailed information may then be obtained about the molecular dynamics. Furthermore, by choosing different wavelengths for the pump and probe pulses, i.e., in a two-color experiment, different sets of energy levels in the vibrational manifold can be excited and probed. The redistribution of electrons within the vibrational manifold is dependent on their position in the energy ladder and thus changes in the pump and probe wavelengths can be used to study the photo-induced dynamics and charge transport in the molecule.

In this paper we report the use of spectrally resolved two-color three-pulse photon echo experiments in the visible spectral range to expand the type of information that can be obtained from time-resolved vibrational spectroscopy. A preliminary account of this work was reported recently in Ref. 10. The experiments allow the study of inter- and intramolecular dynamics in both the ground and excited electronic states and demonstrate the potential of the technique for studying the structural dynamics and interactions in complex molecular systems. This multidimensional form of ultrafast nonlinear coherent spectroscopy should have application in many areas of molecular science, because of the ability to overcome inhomogeneous broadening, remove spectral congestion, and isolate features associated with intramolecular rearrangements.

II. THEORETICAL BACKGROUND

We consider the interaction of pulsed optical radiation with a molecular sample as described in Ref. 1. The polarization induced in an isotropic medium by the radiation can be expressed as a sum of terms involving odd powers of the electric field:

$$\mathbf{P}=\mathbf{P}^{(1)}+\mathbf{P}^{(3)}+\mathbf{P}^{(5)}+\cdots=\mathbf{P}^{(1)}+\mathbf{P}^{\mathrm{NL}}. \tag{1}$$

For three short optical pulses with electric fields E_1, E_2, and E_3 and time delays t_{12} and t_{23} the induced nonlinear optical polarization P^{NL} generates a signal electric field:[3,14]

$$E_s(t)=[4\pi i\omega_s/\Delta \mathrm{k}n(\omega_s)c] \times P^{\mathrm{NL}}(t)\sin(\Delta k\ell/2)\exp(i\Delta k\ell/2), \tag{2}$$

[a]Author to whom all correspondence should be addressed. Electronic mail: dvlap@swin.edu.au

where ℓ is the length of the sample, c the speed of light, Δk the phase-mismatch factor, and $n(\omega)$ the linear refractive index of the sample. Equation (2) is derived in the limit of low optical density and assuming the electric fields are plane waves with slowly varying envelope. Under conditions of perfect phase matching the emitted signal electric field $E_s(t)$ is directly proportional to the nonlinear polarization. In nonlinear spectroscopy of isotropic media the lowest-order optical polarization is the third order. In order to minimize the influence of higher-order terms and interference between the orders the excitation pulses should be of low intensity. Based on response function theory,[1] the third-order nonlinear polarization with wave vector $\mathbf{k}_4=\mathbf{k}_3+\mathbf{k}_2-\mathbf{k}_1$ generated by three pulses with electric fields E_1, E_2, E_3 and frequencies ω_1, ω_2, ω_3 with optical delay lines (constant phase envelope) may be expressed as[15]

$$P^{(3)}(t,t_{12},t_{23}) \approx N(i/\hbar)^3\int_0^\infty dt_3\int_0^\infty dt_2\int_0^\infty dt_1[R_A(t_3,t_2,t_1) + R_B(t_3,t_2,t_1)], \tag{3}$$

where N is the sample concentration. The optical response functions R_A and R_B are given by

$$\begin{aligned} R_A(t_3,t_2,t_1) &= [R_{\mathrm{II}}(t_3,t_2,t_1)+R_{\mathrm{III}}(t_3,t_2,t_1)]E_3(t-t_{23}-t_3) \\ &\times E_2(t-t_3-t_2)E_1^*(t+t_{12}-t_3-t_2-t_1) \\ &\times \exp[-i\omega_3(t-t_{23}-t_3)] \\ &\times \exp[-i\omega_2(t-t_3-t_2)] \\ &\times \exp[i\omega_1(t+t_{12}-t_3-t_2-t_1)], \end{aligned} \tag{4a}$$

$$\begin{aligned} R_B(t_3,t_2,t_1) &= [R_{\mathrm{I}}(t_3,t_2,t_1)+R_{\mathrm{IV}}(t_3,t_2,t_1)]E_3(t-t_{23}-t_3) \\ &\times E_1^*(t-t_{12}-t_3-t_2)E_2(t-t_3-t_2-t_1) \\ &\times \exp[-i\omega_3(t-t_{23}-t_3)] \\ &\times \exp[-i\omega_2(t-t_3-t_2+t_1)] \\ &\times \exp[i\omega_1(t-t_{12}-t_3-t_2)]. \end{aligned} \tag{4b}$$

The processes underlying the third-order nonlinear response functions in Eqs. (4a) and (4b) (R_{I}–R_{IV} and their complex conjugates[1]) may be illustrated by double-sided Feynman diagrams. These diagrams represent the time evolution of the density matrix upon sequential interaction with optical fields and free evolution during the time between the interactions.[1,14] When the generated signals are measured in the phase matching direction $\mathbf{k}_4=\mathbf{k}_3+\mathbf{k}_2-\mathbf{k}_1$, the Feynman diagrams representing the possible three-pulse interactions are as shown in Fig. 1. The time ordering of the interaction occurs with the first interaction at the bottom of the diagram and the signal field at the top. When the first interaction is $\mathbf{k}_1$, the second interaction $\mathbf{k}_2$ can generate a population in the excited state (diagram 2) or the ground state (diagram 3), and the third interaction $\mathbf{k}_3$ allows echo formation through

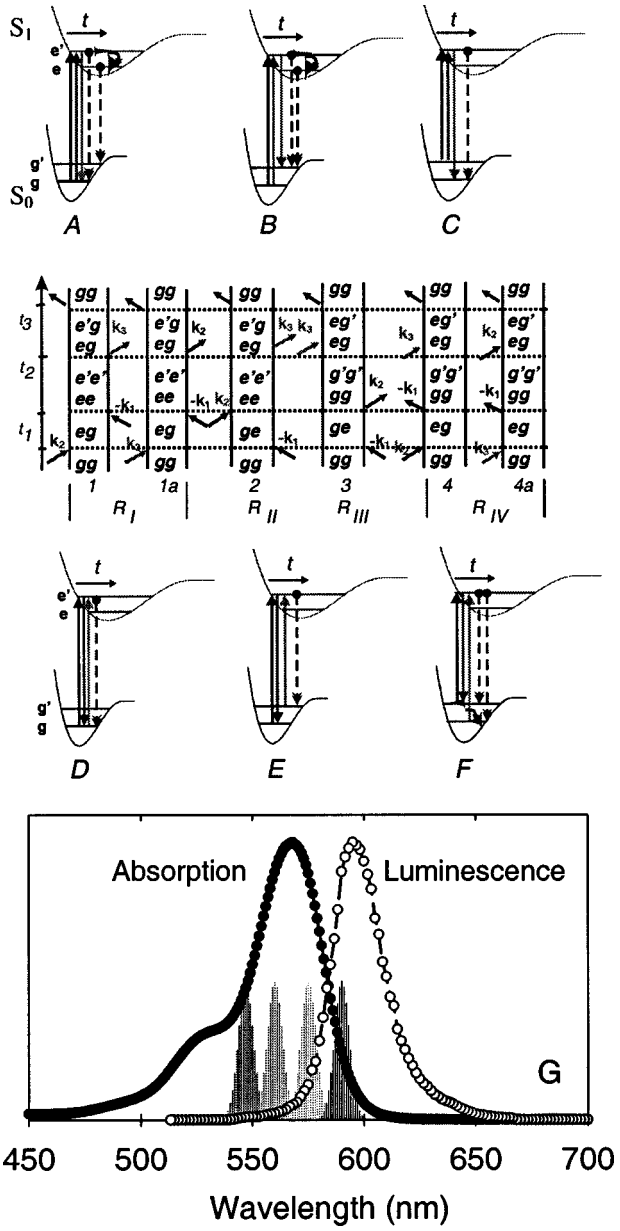

FIG. 1. (i) Feynman diagrams (1–4a) describing the interaction of three pulses with two electronic levels e and g. (The "gg," "$e'g$," etc. represent the density matrices ρ_{gg}, $\rho_{e'g}$, etc.) (ii) Schematic illustration of optical transitions between vibrational levels in two electronic states for generation of vibrational population in excited (A,B,C) and ground (D,E,F) states. (iii) cw absorption and luminescence spectra (G) for 10^{-4} M Rh101 in methanol. The four peaks represent the excitation wavelength used in Fig. 2.

rephasing of the polarization for positive delay times near $t=t_{12}$. The relevant nonlinear response functions are R_{II} and R_{III}. When the first interaction is $\mathbf{k}_2$ (diagrams 1, 4) or $\mathbf{k}_3$ (diagrams 1a, 4a) the first and third interactions have the same phase and the generated signal is a free induction decay (FID). The nonlinear response functions for these pathways are R_{I} and R_{IV}. In the case of an inhomogeneously broadened system the FID would have peaked at negative times; however, as a result of causality only the tail of the FID contribution is observed in an experiment. R_{I} and R_{II} describe the evolution of the excited state population during the population time t_{23} while R_{III} and R_{IV} describe the evolution of the ground state population during t_{23}.

For a two-level system with inhomogeneous broadening given by a Gaussian distribution $G(\omega)=\exp[-(\omega-\omega_{12})^2/\Gamma^2]$ (where Γ is the $1/e$ half-width) the nonlinear response functions are given by[1,16–18]

$$R_{\mathrm{I}}(t_3,t_2,t_1)=R_{\mathrm{IV}}(t_3,t_2,t_1)=\exp[-i\omega_{12}(t_1+t_3)]\exp[-\gamma_{12}(t_1+t_3)]\times\exp[-\gamma_1 t_2]\exp[-\Gamma^2(t_1+t_3)^2/4], \tag{5a}$$

$$R_{\mathrm{II}}(t_3,t_2,t_1)=R_{\mathrm{III}}(t_3,t_2,t_1)=\exp[-i\omega_{12}(t_3-t_1)]\exp[-\gamma_{12}(t_1+t_3)]\times\exp[-\gamma_1 t_2]\exp[-\Gamma^2(t_3-t_1)^2/4], \tag{5b}$$

where ω_{12} is the transition frequency, $\gamma_{12}=1/T_2$ and $\gamma_1=1/T_1$, T_1 is the lifetime of the excited state, and T_2 is the dephasing time of the transition.

When the photon echo signal is recorded with a slow detector, i.e., in a time-integrated measurement, the echo signal may be expressed as

$$S(t_{12},t_{23})\propto\int_0^\infty|P^{(3)}(t,t_{12},t_{23})|^2dt. \tag{6}$$

In such a time-integrated measurement information about the temporal shape of the nonlinear polarization is lost[19] and additional measurements such as time-gated or heterodyne-detected[3] measurements are needed.

An alternative way of obtaining detailed information about the temporal evolution of the nonlinear polarization is to record the echo signal as a function of frequency or wavelength using a spectrometer in a spectrally resolved measurement. The frequency-domain nonlinear polarization is determined by Fourier transformation of the nonlinear polarization with respect to t:

$$\tilde{P}^{(3)}(\omega,t_{12},t_{23})=\int_{-\infty}^{\infty}P^{(3)}(t,t_{12},t_{23})\exp(i\omega t)dt. \tag{7}$$

Fourier transformation of Eq. (3) and including the response functions given by Eqs. (4) and (5) with three delta function laser pulses gives[17]

$$\begin{aligned}\tilde{P}^{(3)}(\omega,t_{12},t_{23})&\propto N\mu_{12}^4\exp[i\omega_3 t_{23}]\exp[-\gamma_1 t_{23}]\\&\times\exp[(i(\omega_{12}-\omega)+\gamma_{12})^2/\Gamma^2)\\&\times\{\exp[-i\omega_{12}(t_{23}-t_{12})]\mathrm{erfc}[i(\omega_{12}-\omega)/\Gamma+\gamma_{12}/\Gamma+t_{12}\Gamma/2]\Theta(t_{12})\Theta(t_{23})+\exp[-i\omega_{12}(t_{23}+t_{12})]\\&\times\exp[-2\gamma_{12}t_{12}]\mathrm{erfc}[i(\omega_{12}-\omega)/\Gamma+\gamma_{12}/\Gamma-t_{12}\Gamma/2]\Theta(-t_{12})\Theta(t_{23})\}\end{aligned} \tag{8}$$

where Θ is the Heaviside function. When the two-level system is excited and probed resonantly we can take $\omega_3=\omega_{12}$.

Under conditions of perfect phase matching and neglecting absorption, the frequency-domain (time-integrated) signal field radiated by this polarization is given by

$$E_s(\omega,t_{12},t_{23})\approx[2\pi i\ell\omega/n(\omega)c]\tilde{P}^{(3)}(\omega,t_{12},t_{23}) \tag{9}$$

and the spectrally resolved photon echo signal is then

$$S_{\mathrm{WPE}}(\lambda_{\mathrm{D}},t_{12},t_{23})\propto|\tilde{P}^{(3)}(\lambda_D,t_{12},t_{23})|^2, \tag{10}$$

where λ_D is the wavelength detected by the spectrometer.

When the first and second pulses temporally overlap in the sample, interference creates a spatially periodic intensity pattern that generates a population grating. For a two-level system, a physical picture based on the scattering of the third pulse from the grating induced by the first two pulses is useful.[20] The spectrum of the scattered signal depends on the spectrum of the probe (third pulse). The detected spectrum can be written in the form

$$S_D(\lambda_D,t_{12},t_{23})=S_{\mathrm{WPE}}(\lambda_D,t_{12},t_{23})+\eta(\lambda_D,t_{12},t_{23})I_{\mathrm{PR}}(\lambda_D), \tag{11}$$

where $\eta(\lambda_D,t_{12},t_{23})$ is the efficiency of the population grating which is proportional to $[\exp(-t_{23}/\tau_{\mathrm{life}})-\exp(-t_{23}/\tau_{\mathrm{rise}})]$, where τ_{life} and τ_{rise} are the lifetime and build-up time of the population grating, respectively, and $I_{\mathrm{PR}}(\lambda_D)$ is the spectral density of the probe pulse.

The time and frequency dependence of $\tilde{P}^{(3)}(\omega,t_{12},t_{23})$ can be sensitive to inhomogeneous broadening and to the vibrational energy spectrum because the different spectral regions can decay with different time constants.[5] We show later that the use of a spectrally resolved measurement in combination with different wavelengths for the pump and probe pulses makes it possible to separate the dynamics of the ground and excited states.

For a simple three-level system with a common ground state, the first pulse creates optical coherence ($\rho_{ge'}$) between the ground state $|g\rangle$ and an excited electronic vibrational state $|e'\rangle$. Vibrational-electronic coupling resulting from anharmonicity of the potential energy surfaces can lead to vibrational coherences $\rho_{ee'}$ in the excited state, which in turn can allow the transfer of the optical coherence ρ_{ge} to the transition $|e\rangle\rightarrow|g\rangle$. An echo signal can then be generated by the third pulse at a frequency corresponding to transitions resonant with the probe frequency ω_{probe} at times near $\omega_{\mathrm{pump}}t_{23}/\omega_{\mathrm{probe}}$ after the third pulse. Vibrational-electronic coupling can also lead to echo signals at frequencies corresponding to optical transitions not resonant with the probe pulse, as described in Ref. 10.

In a three-level system with a common ground or excited state and transition frequencies ω_i, ω_j, there are two different quantum pathways, which can interfere, and the time-integrated signal versus delay time t_{12} or t_{23} can exhibit oscillations (or quantum beats) at the difference frequency $\Delta\omega=|\omega_i-\omega_j|$. In a spectrally resolved measurement, the photon echo signal is detected for those transitions with frequencies equal to the detection frequency of the monochromator ω_D. For the case of coupled oscillators there can be multiple quantum pathways having different initial (ω_j) and final frequencies (ω_i) that lead to the same detection frequency ω_D. The different quantum pathways have different initial frequencies after the second interaction and hence a relative phase difference can evolve between them given by $(\Delta\omega)t_{12}$.[21] This phase difference gives rise to quantum beats

at frequency $\Delta\omega$ in the echo signal as a function of t_{12}. In a spectrally resolved measurement the detection frequency is sharply defined and the beating is more clearly observed because of the smaller number of contributing beat frequencies.

For a multilevel system the polarization results from a summation (approximately)[23] of the nonlinear polarization over n two-level systems:

$$\tilde{P}^{(3)}_{\mathrm{sum}}(\omega,t_{12},t_{23})=\sum \tilde{P}^{(3)}_{n}(\omega,t_{12},t_{23}). \tag{12}$$

In the usual optical Bloch equations the driving terms for the population of the excited state involve the interaction of two independent applied fields (involving the first-order polarization[16,22,23]). The pulse generates coherence between the ground and excited states, which can be transferred between levels. In this case, without considering the detailed interaction of the first two pulses and neglecting the broadening of the coherence during the transfer, we can replace the term $N\mu_{12}^4$ in Eq. (8) with $f_e N\mu_{12}^4$, where f_e is the efficiency of coherence transfer.

There are three time intervals during which the system evolves: the time t_{12} between the first and second interactions, the time t_{23} between the second and third interactions, and the time between the third pulse and the detection time. In a conventional three-pulse photon echo experiment, the time-integrated signal is recorded while one of the two time intervals, t_{12} or t_{23}, is held fixed and the other interval is scanned. This allows control over two delay times. Measurement of the spectrum of the echo signal gives amplitude information at each frequency but the slow detection does not allow the phase to be recorded at each frequency. Complete information about the evolution of the system during the third time interval could be obtained, for example, by mixing the generated signal field with a local oscillator as a function of time (heterodyne detection) or by mixing the signal with a local oscillator in a monochromator (spectral interferometry). However, for the purposes of investigating the dynamics of many molecular processes, the absolute phase of the generated signal is not needed and it is sufficient to spectrally resolve the generated signal. Because there are two distinct time periods that can be scanned, each pulse can be considered to interact separately. This is a useful additional degree of freedom because the number of quantum pathways of the signal that is produced in each situation is different and such a measurement can be helpful for separating the quantum pathways.

III. EXPERIMENT

The femtosecond (fs) laser system consists of a modelocked Ti:sapphire laser and a regenerative amplifier which delivers 80 fs, 1 mJ pulses at a wavelength of 800 nm and a repetition rate up to 1 kHz. The fs beam from the regenerative amplifier is split into two beams for pumping two independent optical parametric amplifiers (OPAs). The two OPAs have several options for frequency generation [second-harmonic generation (SHG), fourth-harmonic generation (FHG) or sum frequency generation (SFG)] allowing the coverage of a broad range of wavelengths (250–2000 nm) with a pulse duration of about 100 fs. The full width at half maximum of the spectral profile of the output of the two OPAs in the SFG option is about 7–10 nm. FROG measurements show a minimal amount of linear chirp in the pulses from the OPAs.

The output of the first OPA is split into two beams, which act as two pump beams ($\mathbf{k}_1$ and $\mathbf{k}_2$), and the output of the second OPA acts as the probe beam ($\mathbf{k}_3$). Three beams with time delays t_{12} and t_{23} and parallel polarizations are aligned in a triangular configuration and focused by a 15 cm focal length lens into the sample. The energy density of each pulse at the sample spot is 1–10 μJ/cm^2. The signal is measured in the phase-matching direction $\mathbf{k}_4=\mathbf{k}_3+\mathbf{k}_2-\mathbf{k}_1$ (or $\mathbf{k}_a=2\mathbf{k}_2-\mathbf{k}_1$ and $\mathbf{k}_b=2\mathbf{k}_1-\mathbf{k}_2$ for the two-pulse experiment) and detected by an Ocean Optics spectrometer with spectral resolution about 2 nm. The spectra are measured at different fixed coherence times t_{12} or population times t_{23} by scanning the other delay time.

The investigated sample is 10^{-4} M Rhodamine 101 (Lamda-Physik) in methanol. The linear absorption and luminescence spectra are shown in Fig. 1G. The maximum of the absorption band occurs at 570 nm and the maximum of the luminescence band at 600 nm.

IV. RESULTS AND DISCUSSION

A. Two-pulse photon echoes

In a two-pulse photon echo experiment the signal is observed in the phase-matching direction $\mathbf{k}_a=2\mathbf{k}_2-\mathbf{k}_1$. The third pulse can be considered to temporally coincide with the second and the Feynman diagrams for this interaction are diagrams 2 and 3 of Fig. 1 with $t_{23}=0$. When the first interaction is $\mathbf{k}_1$ the second interaction $\mathbf{k}_2$ can generate population in the excited state (diagram 2) or the ground state (diagram 3), and the second interaction $\mathbf{k}_2$ allows the creation of an echo. Diagrams A and D (Fig. 1) show the possible interactions of two pulses with the vibrational levels in a simplified four-level system.

Figures 2(a)–2(d) show the echo spectra in the $\mathbf{k}_a$ detection direction versus the delay time between the two pulses for 10^{-4} M Rh101 in methanol at excitation wavelengths of 547, 560, 575, and 590 nm. Zero delay time is defined as the time when the maxima of the two pulses overlap. A peak shift in time (15 fs for 547 nm and 70 fs for 590 nm) of the spectrally integrated signal [closed circles in Figs. 2(a)–2(d)] relative to zero delay time and a redshift of the spectra from the center wavelength of the laser pulses are observed. These shifts increase when the excitation wavelength approaches the wavelength of maximum absorption. The temporal shift in the spectrally integrated photon echo signal results from inhomogeneous broadening in the molecule,[2] while the redshift in the echo spectrum results from a transfer of the optical coherence from the initially excited transition (diagram A in Fig. 1).

B. One-color three-pulse photon echoes

When three pulses with the same wavelength are used, terms corresponding to all six Feynman diagrams in Fig. 1 can contribute to the generated echo signal. Diagrams A and

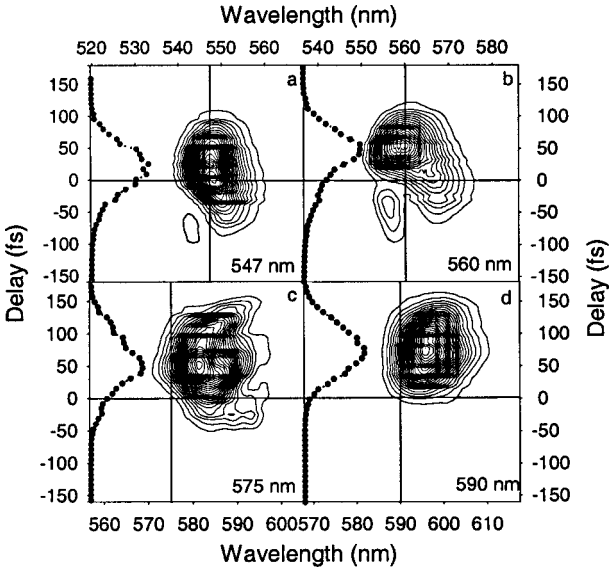

FIG. 2. Contour plot of the spectrum of the two-pulse photon echo in the direction $\mathbf{k}_a = 2\mathbf{k}_2 - \mathbf{k}_1$ vs delay between the pulses for four different laser wavelengths: (a) 547 nm, (b) 560 nm, (c) 575 nm, (d) 590 nm. The dots represent the spectrally integrated echo signal. The laser wavelength is indicated by the vertical line.

D show the possible interactions of three pulses with the vibrational levels. Figure 3 shows contour plots of the spectra of the echo signal in the phase matching direction $\mathbf{k}_4 = \mathbf{k}_3 + \mathbf{k}_2 - \mathbf{k}_1$ versus the population time t_{23} for two cases of the coherence time: $t_{12} = -40$ fs (Fig. 3 diagrams a1–a4) and $t_{12} = +40$ fs (Fig. 3 diagrams b1–b4). The laser wavelengths are 547 nm (Fig. 3 diagrams a1, b1), 560 nm (Fig. 3 diagrams a2, b2), 575 nm (Fig. 3 diagrams a3, b3) and 590 nm (Fig. 3 diagrams a4, b4). For $t_{12} = -40$ fs (diagrams 1 and 4 in Fig. 1) or for negative population times t_{23} (diagrams 1a and 4a in Fig. 1) the FID contribution is expected to be enhanced. In this case the signal intensity is weaker than for $t_{12} = +40$ fs indicating that for this system the FID contribution is smaller than the contribution of the photon echo signal. When the laser wavelength is tuned to the wavelength of maximum absorption (575 nm, Fig. 3 diagrams a3, b3) the spectra exhibit a large redshift and broadening, and some oscillation is observed.

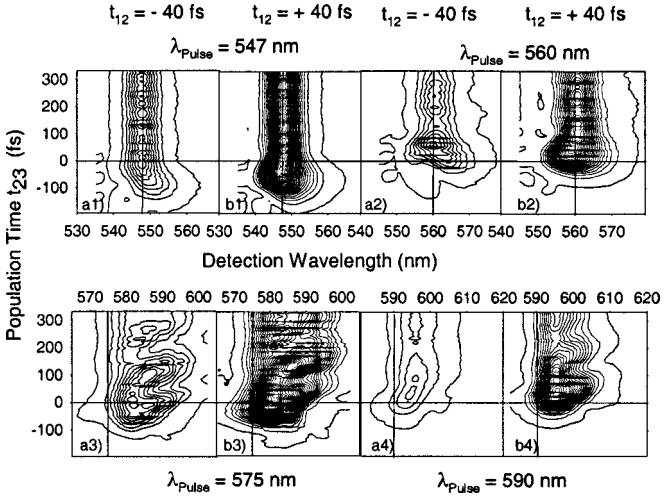

FIG. 3. Contour plot of the spectrum of the one-color three-pulse photon echo in the direction $\mathbf{k}_4 = \mathbf{k}_3 + \mathbf{k}_2 - \mathbf{k}_1$ vs the population time t_{23} for different laser wavelengths (a1, b1: 547 nm; a2, b2: 560 nm; a3, b3: 575 nm; a4, b4: 590 nm) and for different fixed coherence times t_{12} (a1, a2, a3, a4: at -40 fs and b1, b2, b3, b4: at $+40$ fs).

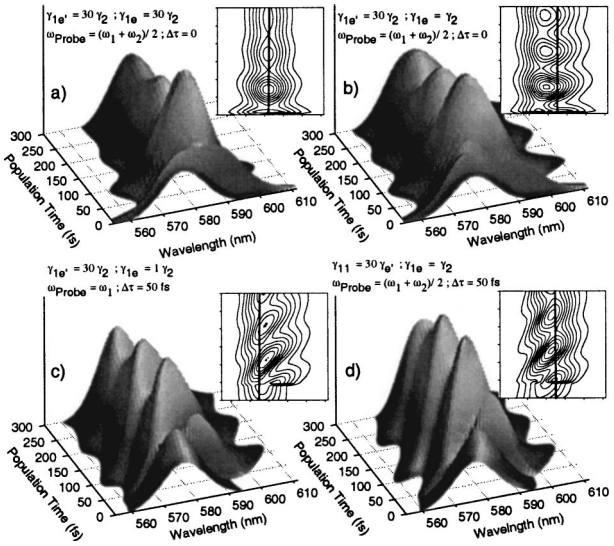

FIG. 4. Simulated photon echo spectrum vs population time t_{23} calculated with Eqs. (8), (11), and (12) for a pair of two-level systems. High frequency $\omega_{ge'} = 17\,391$ cm^{-1} (575 nm), frequency difference $\Delta\omega = 302$ cm^{-1} (10 nm), inhomogeneous width $\Gamma = 0.75\Delta\omega$, dephasing time $\gamma_{12}^{-1} = 6$ ps: (a) $\gamma_{e'}^{-1} = \gamma_e^{-1} = 200$ fs, $\omega_{\text{probe}} = (\omega_{ge'} + \omega_{ge})/2$, $\Delta\tau = 0$; (b) $\gamma_{e'}^{-1} = 200$ fs, $\gamma_e^{-1} = 6$ ps, $\omega_{\text{probe}} = (\omega_{ge'} + \omega_{ge})/2$, $\Delta\tau = 0$; (c) $\gamma_{e'}^{-1} = 200$ fs, $\gamma_e^{-1} = 6$ ps, $\omega_{\text{probe}} = \omega_{ge'}$, $\Delta\tau = 50$ fs; (d) $\gamma_{e'}^{-1} = 200$ fs, $\gamma_e^{-1} = 6$ ps, $\omega_{\text{probe}} = (\omega_{ge'} + \omega_{ge})/2$, $\Delta\tau = 50$ fs.

To apply the theory described by Eqs. (8), (11), (12) we consider a simple two electronic state system with ground state S_0 and excited state S_1 (Fig. 1). The excited state consists of two vibrational levels (e', e) corresponding to two transition modes with frequencies $\omega_{ge'}$ and ω_{ge} $(\omega_{ge'} > \omega_{ge})$. The frequency difference of the two modes is small enough that when the laser frequency is centered at $(\omega_{ge'} + \omega_{ge})/2$ the laser pulse can span the two modes or that when the laser frequency is centered at $\omega_{ge'}$ the optical coherence $\rho_{ge'}$ is generated mostly in the high frequency transition mode and this coherence can be transferred via vibrational-electronic coupling to the lower frequency transition mode with a small change of coherence properties. The coherence transfer is possible because the two vibrational levels are in the same electronic state and have the same dephasing time γ_{12}^{-1} given by the electronic dephasing time but have different population lifetimes $\gamma_{e'}^{-1}$ and γ_e^{-1}.[24] Under such conditions we can apply Eqs. (8) and (12) to a pair of two-level systems that are excited and probed resonantly. The lifetime of the population grating can be treated as the recovery time of the ground state that can be >100 ps in many dye systems.[25]

Figure 4 shows a simulation of two resonant probe modes around 575 nm (17 391 cm^{-1}) when the wavelength difference is 10 nm (302 cm^{-1}). Figure 4(a) is for the case when the wavelength of the probe pulse is mid-way between the two modes and the two modes have the same but very short lifetime $\gamma_{e'}^{-1} = \gamma_e^{-1} = 200$ fs. A broadening of both sides

of the spectrum can be seen at short population times where the photon echo has a large contribution to the observed signal. This simulation corresponds to the case of short excitation wavelengths (<575 nm) (see Fig. 3 diagrams a1–a2 and b1–b2) for which the lifetime of both excited levels is expected to be very short (<200 fs). When the coherence lifetime of the lower excited vibrational level is long (γ_e^{-1} = 6 ps) a broadening of the spectrum on the long wavelength side can be seen [Fig. 4(b)]. Figures 4(c) and 4(d) show the cases when the low frequency mode is delayed by $\Delta\tau$=50 fs relative to the high frequency mode, due to coherence transfer, and when $\omega_{\text{probe}}=\omega_{ge'}$ and $(\omega_{ge'}+\omega_{ge})/2$. These simulations correspond to the case of Fig. 3 diagrams a3–b3 and Fig. 3 diagrams a4–b4, with the laser wavelength tuned to long wavelengths (575 and 590 nm). Diagram A of Fig. 1 illustrates the simulation and gives an explanation of how vibrational relaxation in the excited state can lead to a red-shift of the echo spectrum.

Quantum beat oscillations in the intensity of the echo spectra are observed when the detection wavelength is close to or longer than the maximum of the absorption (Fig. 3 diagrams b3, b4). There are two dominant modes (120 and 220 cm^{-1}) for detection wavelengths of 575 and 580 nm and four modes (120, 220, 330, and 400 cm^{-1}) for a detection wavelength of 600 nm.

C. Two-color three-pulse photon echoes

Two-color photon echo experiments, which allow the variation of the probe wavelength, can lead to the selection of particular transitions. Diagrams B and E in Fig. 1 illustrate the possible transitions between vibrational levels of two electronic states when the pump wavelength is shorter than the probe wavelength, while diagrams C and F show the case when the pump wavelength is longer than the probe wavelength.

For a difference of probe and pump wavelengths of ±15 nm (i.e., larger than the spectral bandwidths of the pulses of ~7 nm) four combinations have been studied for pump and probe wavelengths of 560, 575, and 590 nm. Figure 5 shows the photon echo spectra for two combinations of pump and probe wavelength, at 560 and 575 nm, versus the population time at fixed coherence time $t_{12}=0$ fs [Figs. 5(a) and 5(d)] and versus the coherence time at fixed population times $t_{23}=0$ fs [Figs. 5(b), 5(e)], 140 fs [Fig. 5(c)] and 100 fs [Fig. 5(f)]. Similar spectra are shown in Fig. 6 for two other combinations of pump and probe wavelength, at 575 and 590 nm. In the case when the pump wavelength is longer than 575 nm [Figs. 6(d) and 6(e)] the first interaction only involves transitions from high vibrational levels of the ground state (diagrams C and F in Fig. 1). The spectra measured at each of a range of different coherence times t_{12} and population times t_{23} can give different information because the wavelengths of $\mathbf{k}_2$ and $\mathbf{k}_3$ are not the same.

1. Scans of the population time t_{23} [Figs. 5(a), 5(d) and 6(a), 6(d)]

As in the case of one-color three-pulse experiments, with fixed $t_{12}<0$ there is enhancement of the contribution of the FID and with $t_{12}>0$ the main contribution is the photon

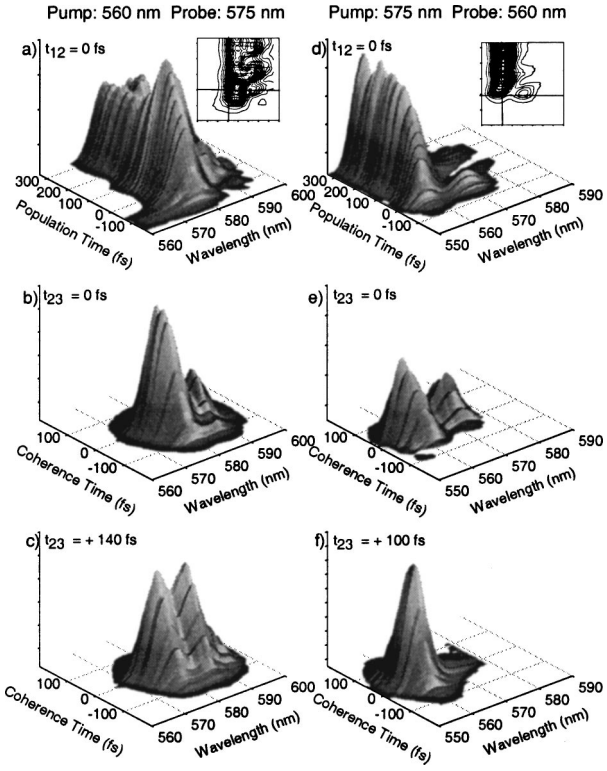

FIG. 5. Two-color three-pulse photon echo spectra vs population time [(a),(d)] and coherence time [(b),(c),(e),(f)] at fixed values of the other delay time for the pump or probe pulse at the absorption maximum (575 nm) and on the blue side (560 nm) of the absorption maximum.

echo. Also, the signal intensity for $t_{12}<0$ is much weaker than for $t_{12}>0$ and the spectral pattern changes only slightly, and therefore we present here only the case for $t_{12}=0$.

When the pump wavelength is 560 nm and the probe 575 nm some oscillations are observed with frequencies of about 160, 210, 320, 440, and 580 cm^{-1}. The oscillations are clearly observed in the intensity versus population time plot with spectral window ~1 nm (Fig. 7) and the frequencies are dependent on the selected detection wavelength. In the spectrally integrated signal versus population time only one oscillation mode (about 260 cm^{-1}) with small visibility can be seen. When the wavelength of the pump and probe are interchanged the oscillation is not observed clearly except at some long wavelengths [around 570 nm—see the inset to Fig. 5(d)].

An advantage of the two-color photon echoes experiment is the observation of vibrational relaxation in real time as shown in Fig. 7 for the case of the probe wavelength at 575 nm. In the two-color experiment an increasing rise time is clearly observed with increasing detection wavelength [Fig. 7(a)] but in the one-color experiment this trend is not observable in the region covered by the laser pulse [Fig. 7(b)]. We define the time difference to reach the maximum at different detection wavelengths as the relaxation time between the corresponding vibrational levels.[10] The vibrational relaxation time increases with detection wavelength at the rate of about 80 fs/5 nm for the case of Rh 101 in methanol.

In the three-pulse two-color photon echo experiment the second pulse creates population in the ground or excited

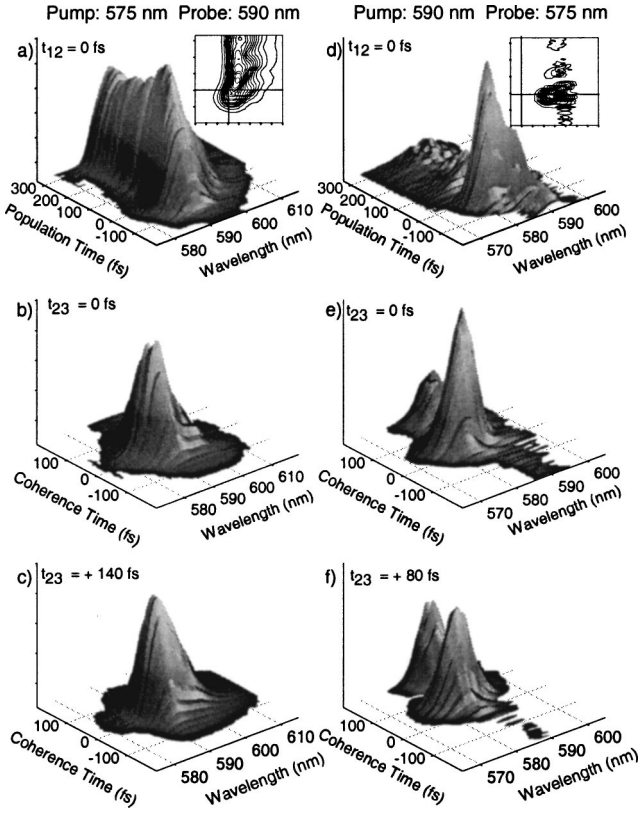

FIG. 6. Two-color three-pulse photon echo spectra vs population time [(a),(d)] and coherence time [(b),(c),(e),(f)] at fixed values of the other delay time for the pump or probe pulse at the absorption maximum (575 nm) and on the red side (590 nm) of the absorption maximum.

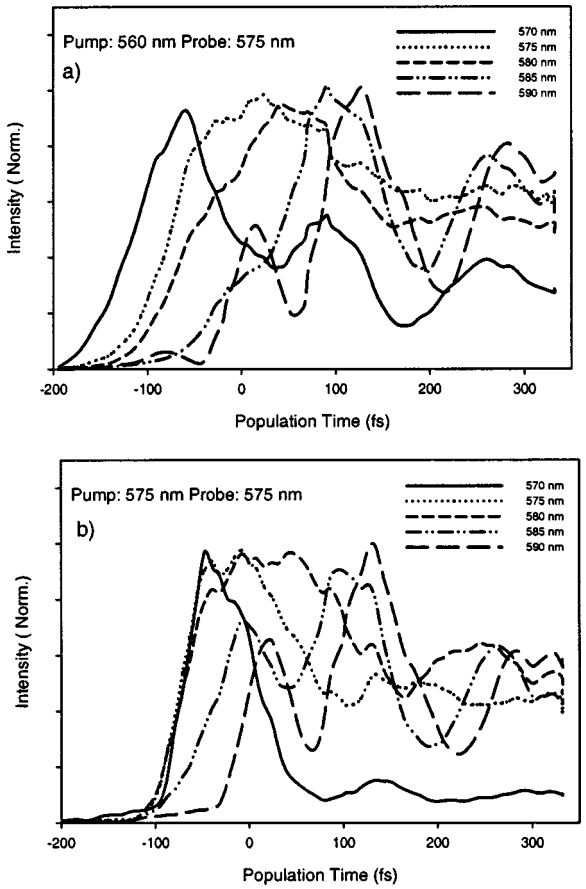

FIG. 7. Spectral density of the photon echo taken with a spectral window of 1 nm for different detection wavelengths of 570, 575, 580, 585, and 590 nm as a function of population time with two different pump wavelengths (a) 560 nm and (b) 575 nm and the same probe wavelength (575 nm).

states ($\rho_{e'e'}$ or $\rho_{g'g'}$) and during the time t_{23} this population ensemble can transfer to lower vibrational levels.

Two extreme cases for the transfer of the population ensemble can be expected.[2] The frequency of the ensemble relative to the mean frequency of the pump pulses is conserved during the transfer and the final frequency distribution is related to the initial frequency distribution, or the coherence transfer randomizes the position within the distribution and the specific final frequency is independent of the initial frequency. In the first case the transfer has a phase memory while in the second case the phase correlation is lost. The third pulse interacts with this ensemble to generate the echo signal and its intensity depends on the degree of phase memory of the efficiency for coherence transfer. For a rigid molecular structure, such as Rh101, we expect a high degree of phase memory. Without considering the details of the coherence transfer by the first two pulses, reflected in the term $f_e N \mu_{12}^2$ in Eqs. (8) and (12), the number of transition modes to be excited can be large. The third pulse which generates the echo signal spans or partially spans the frequency spread of this pulse by interacting with the transition modes. Therefore we can consider a large number of transition modes involved in the resonant excitation and the excitation of the modes can be delayed relative to each other because of the time required for transfer.

Figure 8 shows simulations for the case of three transition modes with the same frequency difference ($\Delta\omega = 260$ cm^{-1}) for time delays between the modes of 80 fs [Fig. 8(a)] and 25 fs [Fig. 8(b)]. Figure 8(a) represents a simulation for coherence transfer in the excited state [Figs. 5(a) and 1(B)] and Fig. 8(b) for coherence transfer in the ground state [Figs. 5(d) and 1(F)]. The short delay of the coherence transfer in the ground state [Figs. 8(b) and 5(d)] can be seen as a result of a broad coherence ensemble in the ground state because of the delocalization of the wave packet in the excited state after excitation and the displacement of the two (S_1,S_0) potential energy surfaces.[26]

2. Scans of the coherence time t_{12} [Figs. 5(b), 5(c), 5(e), 5(f) and 6(b), 6(c), 6(e), 6(f)]

The change of echo intensity for different pump and probe wavelengths reflects the energy relaxation in the relevant vibrational ladder. When the wavelength of the pump is shorter than that of the probe [Figs. 5(b), 5(c) and 6(b), 6(c)] the echo spectrum is enhanced on the long wavelength side at longer population times. This enhancement reflects the dynamics of vibrational relaxation in the excited state, as illustrated in Fig. 1(B). By contrast, when the wavelength of the pump is longer than that of the probe, enhancement of the echo signal occurs on the blue side of the spectrum at longer population times [Figs. 5(e), 5(f) and 6(e), 6(f)] indicating vibrational relaxation in the ground state [Fig. 1(F)]. The spectrum of the vibrational modes shows a splitting due

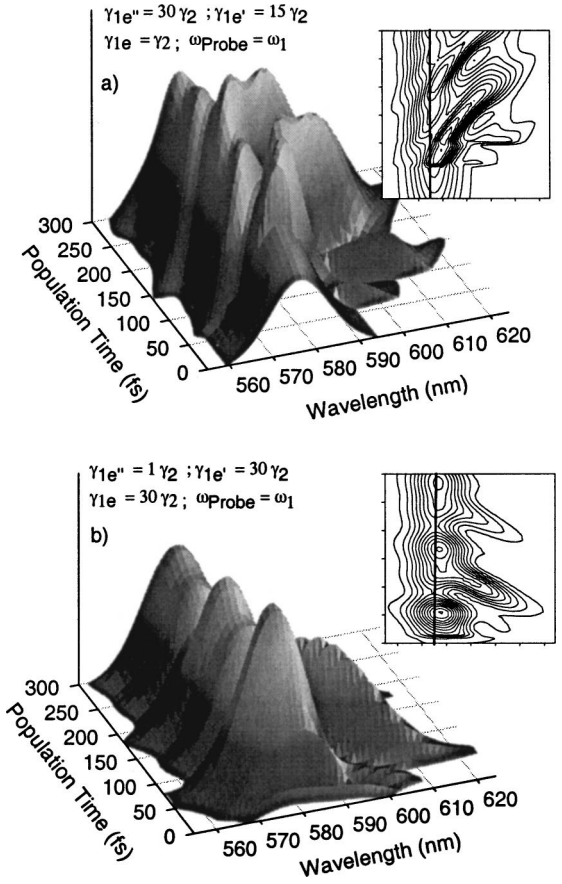

FIG. 8. Simulated photon echo spectrum vs population time t_{23} calculated from Eqs. (8), (11), and (12) for three two-level systems with high frequency $\omega_{ge'}=17\,391\ \mathrm{cm}^{-1}$ (575 nm), frequency difference $\Delta\omega=260\ \mathrm{cm}^{-1}$ (8.6 nm), inhomogeneous width $\Gamma=0.5\Delta\omega$, dephasing time $\gamma_{12}^{-1}=6$ ps (a) $\gamma_{e''}^{-1}=200$ fs, $\gamma_{e'}^{-1}=400$ fs, $\gamma_{e}^{-1}=6$ ps, $\omega_{\mathrm{probe}}=\omega_{ge'}$, $\Delta\tau=80$ fs; (b) $\gamma_{e''}^{-1}=6$ ps, $\gamma_{e'}^{-1}=200$ fs, $\gamma_{e}^{-1}=200$ fs, $\omega_{\mathrm{probe}}=\omega_{ge'}$, $\Delta\tau=25$ fs.

probably to overlapping of the vibrational modes by the spectral bandwidth of the probe pulse. In the case of the probe at 575 nm [Figs. 5(b), 5(c)], two modes are observed which can be fitted by two Gaussians with a splitting of 270 cm^{-1} and width 140 cm^{-1}. The splitting changes with the population time. For a probe wavelength of 560 nm [Figs. 5(e), 5(f)] the splitting is 400 cm^{-1} at short population times ($t_{23}\sim 0$ fs) and 220 cm^{-1} at long population times ($t_{23}\sim 100$ fs).

3. Long scans of the population time t_{23} [Fig. 9]

Figures 9(a)–9(d) show the echo spectrum versus population time for long scans of the population time and a coherence time $t_{12}=0$. For a short probe wavelength (560 nm) the echo spectrum at long population times is similar to the probe spectrum [Figs. 9(a), 9(c)] illustrating the diffraction from the population grating induced in the ground state [Fig. 9(f)], and the coherence ensembles generated by the first two pulses in high vibrational levels of the excited state have a short lifetime. For long probe wavelengths ($\geqslant$575 nm) there is a redshift and broadening of the echo signal [Figs. 9(b), 9(d)] due to transitions from lower vibrational levels of the excited state that decay with a lifetime of around 10 ps [Fig. 9(e)] which is the lifetime of the coherence ensemble.

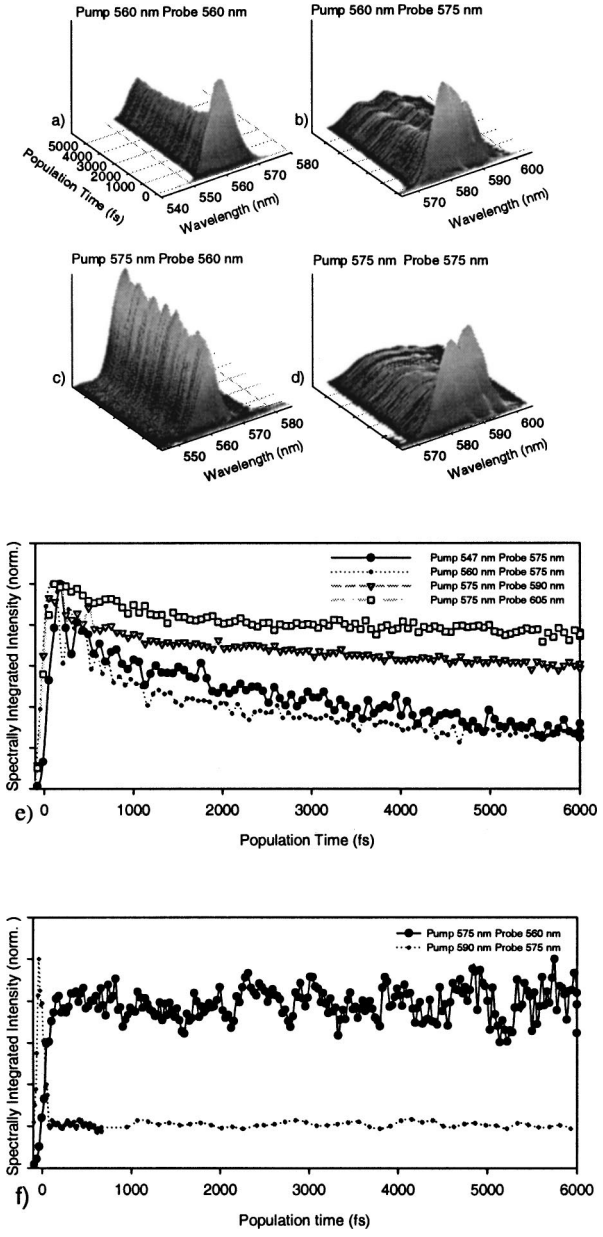

FIG. 9. Two-color three-pulse photon echo spectra vs population time t_{23} up to 6 ps [(a)–(d)] for $t_{12}=0$ and the spectrally integrated signal plots [(e),(f)] for different combinations of the pump and probe wavelength [(e) $\lambda_{\mathrm{probe}}>\lambda_{\mathrm{pump}}$, (f) $\lambda_{\mathrm{probe}}<\lambda_{\mathrm{pump}}$].

V. CONCLUSIONS

We have investigated the technique of spectrally resolved two-color three-pulse photon echoes and applied it to the study of the dynamics of vibrational electronic states of the dye molecule rhodamine 101 in methanol. The spectrally resolved photon echo signals yield information on the temporal evolution of the third-order nonlinear polarization and thus provide more information than is available from spectrally integrated techniques such as the photon echo peak shift method. The photon echo spectra are found to be strongly dependent on the wavelengths of the pump and probe pulses, demonstrating the potential of the technique for studying the dynamics of both the ground state and the excited state of complex molecules.

ACKNOWLEDGMENT

We thank Barbara McKinnon for valuable discussions about the theory of photon echoes. This project was supported by a stategic initiative grant from Swinburne University of Technology and a Discovery Grant from the Australian Research Council.

[1] S. Mukamel, *Principles of Nonlinear Optical Spectroscopy* (Oxford University Press, New York, 1995).
[2] R. Agarwal, B. S. Prall, A. H. Rizvi, M. Yang, and G. R. Fleming, J. Chem. Phys. **116**, 6243 (2002), and references therein.
[3] W. P. de Boeij, M. S. Pshenichnikov, and D. A. Wiersma, Chem. Phys. **233**, 287 (1998), and references therein.
[4] J. D. Hybl, A. A. Ferro, and D. M. Jonas, J. Chem. Phys. **115**, 6606 (2001).
[5] M. C. Asplund, M. Lim, and R. M. Hochstrasser, Chem. Phys. Lett. **323**, 269 (2000).
[6] D. E. Thompson, K. A. Merchant, and M. D. Fayer, J. Chem. Phys. **115**, 317 (2001), and references therein.
[7] C. Scheurer and S. Mukamel, J. Chem. Phys. **115**, 4989 (2001).
[8] L. D. Book, A. E. Ostafin, N. Ponomarenko, J. R. Norris, and N. F. Scherer, J. Phys. Chem. B **104**, 8295 (2000).
[9] T.-S. Yang, M.-S. Chang, R. Chang, M. Hayashi, S. H. Lin, P. Vöhringer, W. Dietz, and N. F. Scherer, J. Chem. Phys. **110**, 12070 (1999).
[10] L. V. Dao, C. Lincoln, M. Lowe, and P. Hannaford, Physica A **327**, 123 (2003).
[11] S. Mukamel, A. Piryatinski, and V. Chernyak, Acc. Chem. Res. **32**, 145 (1999).
[12] A. Tokmakoff, A. S. Kwok, R. S. Urdahl, R. S. Francis, and M. D. Fayer, Chem. Phys. Lett. **234**, 289 (1995).
[13] A. Tokmakoff, M. J. Lang, X. J. Jordanides, and G. R. Fleming, Chem. Phys. **233**, 231 (1998).
[14] Y. R. Shen, *The Principles of Nonlinear Optics* (Wiley-Interscience, New York, 1984).
[15] A. W. Albrecht, J. D. Hybl, S. M. Sarah, S. M. G. Feader, and D. M. Jonas, J. Chem. Phys. **111**, 10934 (1999).
[16] S. M. G. Feader and D. M. Jonas, J. Phys. Chem. A **103**, 10489 (1999).
[17] J. Erland, V. G. Lyssenko, and J. M. Hvam, Phys. Rev. B **63**, 155317 (2001).
[18] C. Crepin, Phys. Rev. A **67**, 013401 (2003).
[19] W. P. de Boeij, M. S. Pshenichnikov, and D. A. Wiersma, J. Phys. Chem. **100**, 11806 (1996).
[20] J. D. Hybl, A. W. Albrecht, S. M. G. Feader, and D. M. Jonas, Chem. Phys. Lett. **297**, 307 (1998).
[21] K. A. Merchant, D. E. Thompson, and M. D. Fayer, Phys. Rev. A **65**, 023817 (2002).
[22] W. Wegener, D. S. Chemla, S. Schmitt-Rink, and W. Schafer, Phys. Rev. A **42**, 5675 (1990).
[23] J. M. Shacklette and S. T. Cundiff, Phys. Rev. B **66**, 045309 (2002).
[24] P. Vöhringer, D. C. Arnett, R. A. Westervelt, M. J. Feldstein, and N. F. Scherer, J. Chem. Phys. **102**, 4027 (1995).
[25] O. Marcano, N. Melikechi, and G. Verde, J. Chem. Phys. **113**, 5830 (1999).
[26] W. T. Pollard, S. L. Dexheimer, Q. Wang, L. A. Peteanu, C. V. Shank, and R. A. Mathies, J. Phys. Chem. **96**, 6147 (1992).